Available online at www.sciencedirect.com
SCIENCE DIRECT®
ELSEVIER
Nuclear Instruments and Methods in Physics Research B 216 (2004) 407–413
NIM B
Beam Interactions with Materials & Atoms
www.elsevier.com/locate/nimb

Direct ion beam synthesis of II–VI nanocrystals

U.V. Desnica [a,*], M. Buljan [a], I.D. Desnica-Frankovic [a], P. Dubcek [a], S. Bernstorff [b], M. Ivanda [a], H. Zorc [a]

[a] *Department of Physics, Rudger Boskovic Institute, Bijenicka 54, 10000 Zagreb, Croatia*
[b] *Sincrotrone Trieste, SS 14 km163,5, 34012 Basovizza, Italy*

Abstract

We have studied the direct synthesis of nanoparticles formed by dual implantation of large and equal doses of Cd + S, Zn + Te, Cd + Te or Pb + Te ions into SiO_2 substrate. Grazing incidence small angle X-ray scattering (GISAXS), transmittance measurements and Raman spectroscopy were used to investigate implanted composites. The 2D GISAXS patterns suggest the synthesis of nanoparticles already during ion implantation, performed either at 300 or at 77 K, while annealing at higher T causes an increase of the fraction and the average size of synthesized nanoparticles. After high-T annealing both optical methods detected nanocrystals of compound semiconductors CdS, ZnTe or CdTe through the appearance of the respective first optical gaps, E_g, in transmittance measurements and characteristic LO peaks in Raman spectra. It is proposed that at high ion doses a fraction of implanted atoms synthesize already during implantation into amorphous aggregates of compound semiconductor, which transform into crystalline nanoparticles after annealing.

PACS: 61.10.Eq; 81.07.−b; 61.72.V; 61.46.+w; 81.20.−n; 81.05.Ys
Keywords: Nanocrystals; Implantation; GISAXS; Raman; Transmittance; CdS; CdTe; ZnTe; PbTe; Quantum dots

1. Introduction

There is an intense interest and strong research activity going on to develop technology for the efficient and well reproducible synthesis of nanoparticles (NPs) [1–4]. Control over the particle size enables strong modifications of electronic, optical and other properties of NPs, offering a number of potential applications in semiconductor and other industries [1]. The main interest in wide band-gap semiconductors NPs comes out from the pronounced effects of quantum confinement – strongly dependent on the particle size – which make possible the tunability of the band-gap and of the powerful visible photoluminescence. Sequential implantation of equal doses of constituent atoms offers a unique way to produce compound-semiconductor NPs [1,3–6]. In this paper the synthesis of NPs of a number of binary semiconductors by high dose ion implantation was investigated by means of grazing incidence small angle X-ray scattering (GISAXS), transmittance measurements and Raman spectroscopy.

* Corresponding author. Tel.: +385-1-4561-173; fax: +385-1-4680-114.
E-mail address: desnica@rudjer.irb.hr (U.V. Desnica).

0168-583X/$ - see front matter
doi:10.1016/j.nimb.2003.11.068

2. Experimental details

Samples were produced by implanting equal doses of metal ions (Cd, Zn or Pb) and chalcogen ions (S or Te) into amorphous SiO_2 (fused silica, Corning 7940). All ions were singly charged and ion rates were close to 25 μA/cm^2. Ion doses were 4×10^{16} cm^{-2} of each type of ions in all samples, except for CdS samples, where doses were 10^{17} cm^{-2} (Table 1). Samples nos. 1–4 were implanted at room temperature (RT) and samples (5–10) at liquid nitrogen temperature (LN2). Half of the samples (even numbers in Table 1) were subsequently annealed at high annealing temperature ($T_a = 1073$ or 1273 K) in the flow of Ar + 4%H_2 for 1 h (except sample no. 4, which underwent rapid thermal annealing for 16 min. Ion energies were selected using SRIM calculations to create similar, overlapping concentration profiles of metal and chalcogen ions. Doses, ion energies, temperatures of implantation, T_i, and temperatures of annealing, T_a, are given in Table 1 for all samples. SRIM-calculated peak-volume concentrations of each of implanted atoms were in range $6–8\times10^{21}$ cm^{-3} at depth of 60–70 nm (exemptions were samples 1 and 2, for which both implant doses and maximum-depth positions were approximately twice as large). For sample #1 the overlapping of depth profiles of Cd and S atoms was experimentally confirmed using Rutherford back scattering, with concentration's maxima being around 6.3×10^{21} cm^{-3}, at depth of 130 nm.

GISAXS experiments were carried out with the X-ray wavelength, $\lambda = 0.154$ nm, at the Austrian SAXS beamline at Elettra, Sincrotrone Trieste, Italy [7]. The GISAXS patterns were recorded with

Table 1
List of all samples, including their number, name, ion doses and energies for each ion, implantation temperatures, T_i, and annealing temperatures, T_a, if any, as well as calculated values of the average diameter, R, and the interparticle distance, L, of nanocrystals, as obtained from the LMA analysis

Sample no.	Sample name	Doses (ions cm^{-2})	Implantation energy (keV)	T_i K^{-1} T_a K^{-1}	R (nm) $\pm\Delta R$ (nm)	L (nm) $\pm\Delta L$ (nm)
1	CdS1	Cd(1E17) S(1E17)	Cd(320) S(115)	RT –	1.85 0.03	7.95 0.1
2	CdS2	Cd(1E17) S(1E17)	Cd(320) S(115)	RT 1073	2.07 0.03	7.2 0.09
3	ZnTe3	Zn(4E16) Te(4E16)	Zn(115) Te(190)	RT –	2.41 0.01	8.8 0.03
4	ZnTe4	Zn(4E16) Te(4E16)	Zn(115) Te(190)	RT 1073	2.55 0.03	9.12 0.05
5	ZnTe5	Zn(4E16) Te(4E16)	Zn(110) Te(160)	LN2 –	2.49 0.02	9.33 0.05
6	ZnTe6	Zn(4E16) Te(4E16)	Zn(110) Te(160)	LN2 1273	3.03 0.02	13.2 0.06
7	CdTe7	Cd(4E16) Te(4E16)	Cd(155) Te(160)	LN2 –	2.2 0.02	8.57 0.05
8	CdTe8	Cd(4E16) Te(4E16)	Cd(155) Te(160)	LN2 1273	3.42 0.02	11.3 0.06
9	PbTe9	Pb(4E16) Te(4E16)	Pb(210) Te(160)	LN2 –	2.05 0.011	7.5 0.02
10	PbTe10	Pb(4E16) Te(4E16)	Pb(210) Te(160)	LN2 1273	3.54 –	13.2 –

ΔR and ΔL denote estimated errors in R and L, respectively. RT denotes room temperature and LN2 the temperature of liquid nitrogen (77 K).

1024×1024 pixels 2D CCD-detector, placed in the plane perpendicular to the specular plane, at the distance of 200 cm from the sample. Spectra where first corrected for background intensity and detector response, and then for refraction and absorption effects [8]. Transmittance measurements were done using the Perkin Elmer UV/VIS spectrometer lambda 25, while Raman spectra were taken using the triple spectrometer (DILOR Z-24), excitation line of 2.57 eV from an Ar-ion laser.

3. Results

3.1. GISAXS results

Fig. 1 shows 2D GISAXS patterns for investigated samples. Left panes of Fig. 1 (odd numbers) represent patterns from as-implanted samples, while spectra presented on the right side refer to samples annealed at high temperatures (even numbers). The 2D patterns represent maps of the scattering intensities in reciprocal space, q (wave

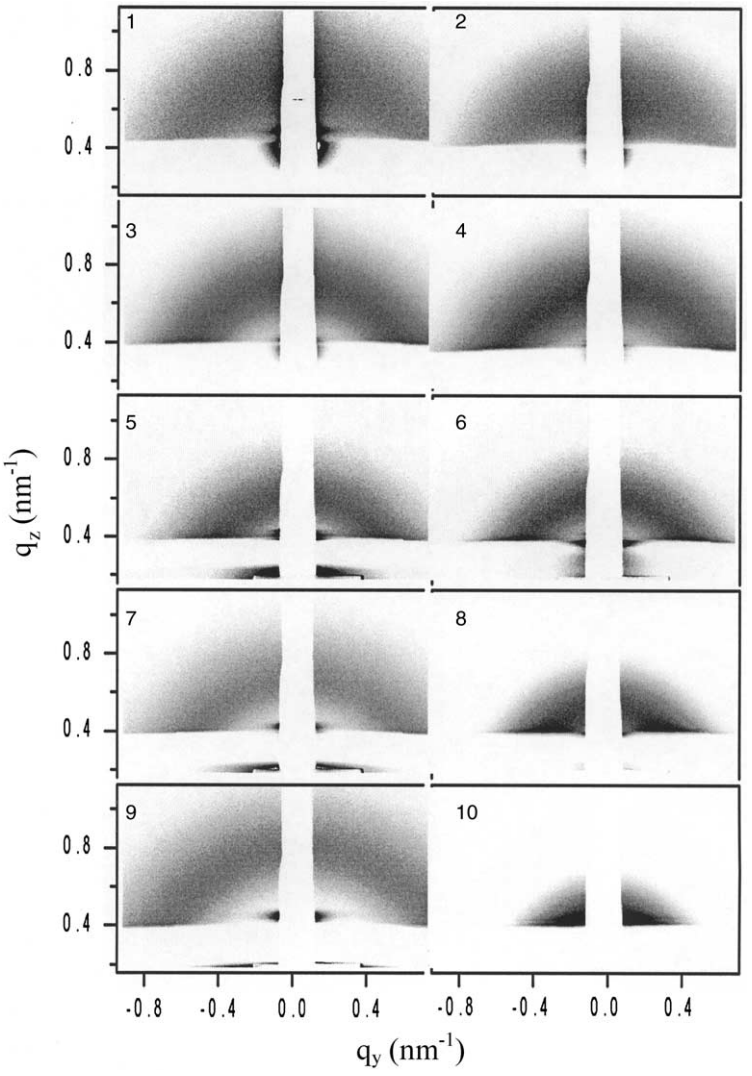

Fig. 1. Two-dimensional GISAXS patterns of double-species ion implanted SiO_2. Numbers $1, 2, \ldots, 10$ refer to samples from Table 1.

vector $q = (4\pi/\lambda)\sin\beta$, 2β being the scattering angle). An inserted beam stopper blocks strong surface signals in/close to the specular plane (reflected beam, Yoneda, etc.), permitting better sensitivity for the weak diffuse scattering at larger q. The incidence angle of the X-ray beam, α_i, used during measurements presented in Fig. 1 was $\alpha_i = \alpha_c + 0.05°$, where α_c denotes the critical angle for total external reflection. For this angle of incidence the penetration depth corresponds roughly to, or close to the maximal volume density of the implanted atoms. All GISAXS patterns in Fig. 1 comprise a highly intense region close to the center (remaining part of surface contributions, which are not relevant for further discussion) and pronounced half rings. GISAXS patterns of non-implanted SiO_2 (not shown) is substantially different, comprising only the reflected signal in the specular plain. The presented rings are circular and generally similar in shape in all directions. In all annealed samples (right) rings were of relatively stronger intensity and of smaller radius than in respective non-annealed samples.

Comparative 1D scattering intensity profiles, $I(q)$, taken along the polar angle = 70° from some of the 2D spectra in Fig. 1, are shown in Fig. 2. The annealing at high temperature causes a shift of the intensity maximum toward lower q as well as somewhat steeper decrease of $I(q)$ on the right side of the peak maximum.

Spectra were analyzed using either simple particle scattering model (Guinier approximation) or local mono-disperse approximation (LMA) [9]. Numerical results obtained from LMA for the average aggregate radius, R, and for the average distance among NPs, L, are shown in Table 1. Values achieved from Guinier approximation were quite similar. GISAXS results suggest that a considerable fraction of NPs has been synthesized already during implantation.

3.2. Optical characterization

Results of transmittance (TR) measurements on samples from Fig. 2 are shown in Fig. 3. In all annealed samples there is a distinct 'kink' in the TR curves at energies corresponding to the first energy gap, E_g, of the respective semiconductor.

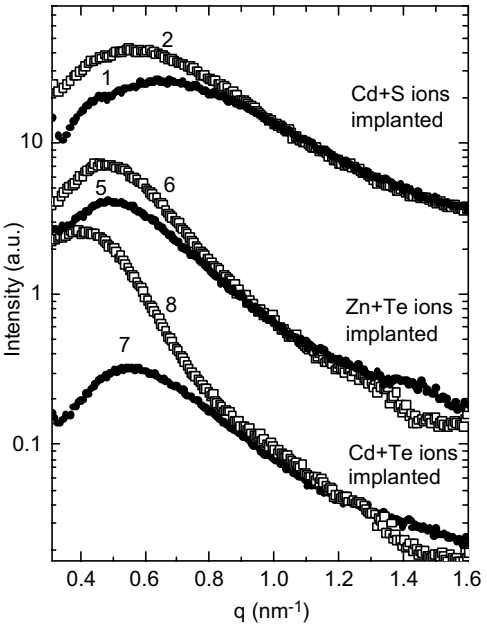

Fig. 2. 1D intensity profiles from the 2D spectra shown in Fig. 1, taken along the detector polar angle $\phi = 70°$. Numbers $1, 2, \ldots, 8$ refer to samples from Table 1.

Result suggests that in all three annealed samples (CdS2, ZnTe6 and CdTe8), some of the implanted ions synthesized into compound semiconductors. Changes in the TR are better perceived in the first derivative of TR (Fig. 3(b)). The maximum of the peak position corresponds to the E_g of the respective semiconductor nanocrystals [10,11]. There is a shift of the peak maxima towards higher energies ('blue shift') in comparison to bulk values for respective E_g, reflecting quantum confinement of isolated semiconductor nanocrystals formed in an insulating, amorphous matrix. However, for non-annealed samples, analogous changes in TR (and its first derivative) are completely absent.

Examples of Raman data are shown in Fig. 4 for the same set of samples. Presented Raman spectra are obtained after the subtraction of the wide background signal originating from the amorphous SiO_2. Distinct lines around 170 cm^{-1} for sample CdTe8, close to 205 cm^{-1} for ZnTe6 and around 295 cm^{-1} for CdS2 were found, respectively. These signals can be confidently

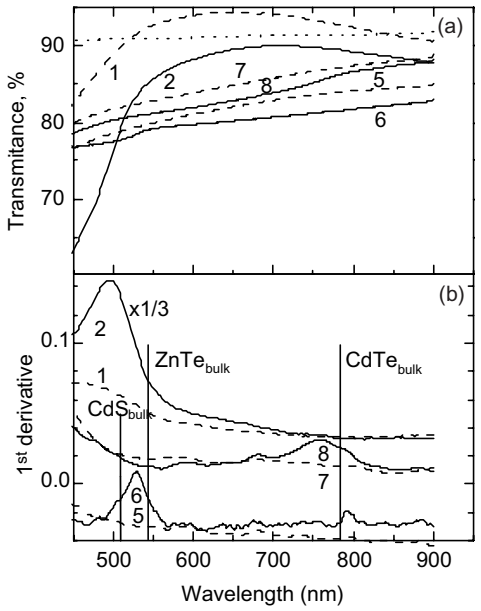

Fig. 3. Optical transmission spectra (a), and their first derivative (b), of three types of as-implanted samples (dashed lines) and implanted + annealed samples (full lines): 1 = CdS1, 2 = CdS2, 5 = ZnTe5, 6 = ZnTe6, 7 = CdTe7, 8 = CdTe8. Ion doses and energies are given in Table 1. The transmittance of SiO_2 is also shown (dotted line in (a)). The bulk values of gap energy E_g for CdS, CdTe and ZnTe are indicated in (b).

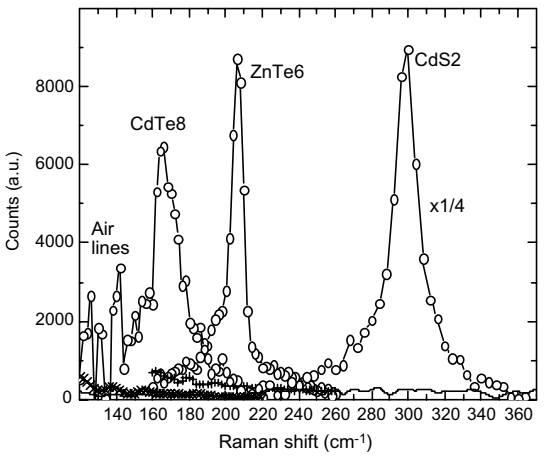

Fig. 4. Raman spectra of samples 1 = CdS1, 2 = CdS2, 5 = ZnTe5, 6 = ZnTe6, 7 = CdTe7, 8 = CdTe8, using the 2.41 eV excitation line.

assigned to longitudinal optical (LO) peaks, expected for crystalline CdTe, ZnTe and CdS semiconductors, respectively. Hence, Raman results confirm the synthesis of implanted constituent ions into semiconductors after high-temperature annealing. Again, like with the (non)appearance of characteristic E_g in transmittance results, there is no positive sign of well-defined inter-atomic bonds, characteristic for respective crystalline semiconductors (no LO peaks) in spectra of as-implanted samples CdS1, ZnTe5 and CdTe7.

4. Discussion

GISAXS has been recently successfully applied to study nanoparticles embedded in matrices with low electron density, including NPs obtained by ion implantation [6,12]. Studied NPs consisted of either single metal atoms, (Au, Ag, Fe, Pt, Co, ...) [9,13,14] or metal alloy (Cu–Ni) NPs [12] or binary semiconductors (CdS, ZnTe, ZnS) [4–6,15,16]. In implanted samples, in principle, nanoparticles can be observed by GISAXS when atoms, implanted uniformly into the substrate, become de-mixed and aggregated into nanoparticles. Spontaneous clustering is usually induced and controlled by thermal treatment. If nanoparticles are spatially correlated, a characteristic 'halo' (ring-like shape) is observed in 2D GISAXS pattern [9,13–16], which is circular if NPs are distributed isotropically. Generally, the appearance of a 'ring' in GISAXS pattern is considered as a sure sign of successful synthesis of nanoparticles in the nm size-range [13–17]. The size of NPs, as well as their shape, were in numerous cases compared with sizes/shape determined from the cross-sectional TEM analysis, and satisfactory agreements between the two methods were, generally, observed [9,13–17], confirming that the GISAXS signal indeed corresponds to synthesized nanoparticles and reflects their properties.

Hence, the presented GISAXS results (Figs. 1 and 2) reveal that some NPs are synthesized in all studied samples: not only in annealed ones but also in as-implanted samples, even when the implantation was done at LN2 temperature (samples 5–10).

Annealed samples: Both optical methods confirmed that after high-T annealing (at least part) of

the implanted Cd + S, Zn + Te or Cd + Te ions synthesize into nanocrystals of the respective binary semiconductor – CdS, ZnTe or CdTe. This finding agrees well with a recent study of Cd + S implanted samples, in which, after annealing at 1273 K, for a range of ion doses CdS nanocrystals were detected by several methods [3]. For these CdS NPs the GISAXS-determined size and size distribution of NPs [16] agreed very well with sizes/size distribution determined from TEM [3] as well as with sizes determined from the blue shift of E_g in TR [3].

As-implanted samples: The intensity of the NPs-related GISAXS signals, at least for samples implanted with Cd + S or Zn + Te (Fig. 2), is similar for as-implanted and annealed ones. Consequently, the quantity of clustered material should be comparable in both cases. For these same samples the LMA analysis gave the percentages of synthesized implanted ions of about 40% and 60% before and after annealing, respectively. Complete lack of characteristic signal in TR (particularly in its first derivative, Fig. 3(b)), and particularly complete lack of the LO peak in Raman signals (Fig. 4), clearly show that nanoclusters in as-implanted samples do not consist of crystalline semiconductor phase. A question arises what is the chemical nature of NPs observed by GISAXS in as-implanted samples. One possibility is that GISAXS-observed NPs are single-species, metal clusters. This hypothesis implies that at some T_a these metal NPs would dissolve while the other kind of nanoparticles (compound semiconductor CdS, ZnTe, CdTe) would form. However, in a recent detailed comparative studies of a series of samples implanted with the same high dose of Cd and S ions (10^{17} cm^{-2} each), but annealed at different temperatures in the $T_a = \text{RT}$ to $= 1173$ K range, a set of very smoothly changing GISAXS spectra was obtained [6]. Only small, gradual increase of average particle size was observed with each T_a step. There was not any discontinuity or other change that would suggest that one sort of nanoparticles (i.e. Cd clusters) is transforming into another (CdS NPs). The other possibility is that the high-dose implantation, at RT or lower temperatures, creates small-size clusters of compound semiconductor material but in the amorphous phase. Such amorphous aggregates would be equally well observable by GISAXS but features characteristic for the crystalline phase of semiconductor would be absent in TR and Raman spectra. Obtaining amorphous aggregates with high-dose, low-T implantation would be consistent with the findings of some other methods of NPs synthesis, where small amorphous aggregates were obtained in low-T non-equilibrium deposition processes, and the crystallization into NPs was achieved only after subsequent thermal processing [18,19]. Very little is known about NPs directly produced by implantation, since practically all published data refer to NPs obtained only after high-T annealing. Hence, further characterization of directly synthesized NPs in as-implanted samples is needed.

5. Conclusions

Direct synthesis of nanoparticles formed by dual implantation of large and equal doses of Cd + S, Zn + Te, Cd + Te or Pb + Te ions into SiO_2 substrate was studied. Grazing incidence small angle X-ray scattering (GISAXS), Transmittance measurements and Raman spectroscopy were used to investigate implanted composites. The 2D GISAXS patterns suggest the synthesis of nanoparticles already during ion implantation either at RT or at LN2 temperature, while annealing at higher T_a caused an increase of the fraction and the average size of synthesized nanoparticles. In all cases an isotropically distributed 3D ensemble of these nanoparticles in the amorphous SiO_2 was established. After high-T annealing both optical methods detected nanocrystals of compound semiconductors CdS, ZnTe, or CdTe through the appearance of the respective first optical gaps, E_g, in transmittance measurements and characteristic LO peaks in Raman spectra. The chemical nature of nanoparticles observed by GISAXS in as-implanted samples remains to be determined. A hypothesis is put forward that at high ion doses a fraction of implanted atoms synthesize already during implantation into amorphous aggregates of

compound semiconductor, which transform into crystalline nanoparticles after annealing.

Acknowledgements

We thank C.W. White, A. Meldrum and H. Karl for providing implanted samples. This work was supported by the Ministry of Science and Technology, Republic of Croatia.

References

[1] A. Meldrum, R.F. Haglund Jr., L.A. Boatner, C.W. White, Adv. Mater. 13 (2001) 1431.
[2] J.D. Budai, C.W. White, S.P. Wiothrow, M.F. Chisholm, J. Zhu, R.A. Zuhr, Nature 390 (1997) 384.
[3] C.W White, A. Meldrum, J.D. Budai, S.P. Withrow, E. Sonder, R.A. Zuhr, D.M. Hembree Jr., M. Wu, D.O. Henderson, Nucl. Instr. and Meth. B 148 (1999) 991.
[4] H. Karl, I. Grosshans, W. Attenberger, M. Schmid, B. Stritzker, Nucl. Instr. and Meth. B 178 (2001) 126.
[5] U.V. Desnica, I.D. Desnica-Frankovic, O. Gamulin, C.W. White, E. Sonder, R.A. Zuhr, J. Non-Cryst. Solids 299–302 (2002) 1100.
[6] U.V. Desnica, P. Dubcek, I.D. Desnica-Frankovic, M. Buljan, S. Bernstorff, S.W. White, J. Appl. Cryst. 36 (2003) 443–446.
[7] H. Amenitsch, S. Bernstorff, M. Kriechbaum, D. Lombardo, H. Mio, M. Rappolt, P. Laggner, J. Appl. Cryst. 30 (1997) 872.
[8] M. Buljan, K. Salamon, P. Dubcek, S. Bernstorff, I.D. Desnica-Frankovic, O. Milat, U.V. Desnica, Vacuum 71 (2003) 65.
[9] D. Babonneau, I.R. Videnovic, M.G. Garnier, P. Oelhafen, Phys. Rev. B 63 (2001) 195401.
[10] B.G. Potter Jr., J.H. Simmons, J. Appl. Phys. 68 (1990) 1218.
[11] M. Sotelo-Lerma, M.A. Quevedo-Lopez, R.A. Orozco-Teranm, R. Ramirez-Bon, F.J. Espinoza-Beltran, J. Phys. Chem. Solids 59 (1988) 145.
[12] E. Cattaruzza, F. d'Acapito, F. Gonella, A. Longo, A. Martorana, G. Mattei, C. Maurizio, D. Thiaudiere, J. Appl. Cryst. 33 (2000) 740.
[13] D. Babonneau, A. Naudon, D. Thaudiere, S. Lequien, J. Appl. Cryst. 32 (1999) 226.
[14] A. Naudon, D. Thiaudiere, J. Appl. Cryst. 30 (1997) 822.
[15] I.D. Desnica-Frankovic, U.V. Desnica, P. Dubcek, M. Buljan, S. Bernstorff, H. Karl, I. Großhans, B. Stritzker, J. Appl. Cryst. 36 (2003) 439.
[16] U.V. Desnica, P. Dubcek, I.D. Desnica-Frankovic, M. Buljan, K. Salamon, O. Milat, S. Bernstorff, C.W. White, Nucl. Instr. and Meth. B 200 (2003) 191.
[17] J.R. Levine, J.B. Cohen, Y.W. Chung, P. Georgopoulos, J. Appl. Cryst. 22 (1989) 528.
[18] R. Ramirez-Bon, F.J. Espinoza-Beltran, H. Arizpe-Chavez, O. Zelaya-Angel, F. Sanchez-Sinencio, J. Appl. Phys. 77 (1995) 5461.
[19] Ch. Ye, G. Meng, Y. Wang, Z. Jiang, L. Zhang, J. Phys. Chem. B 106 (2002) 10338.